ARL-TR-9567 ● SEP 2022

DEVCOM ARMY RESEARCH LABORATORY

The T5 Isochronal Age-Hardening Response of As-Solidified Mg–Li–RE–(Al) Alloys

by Taylor Cain and Joseph Labukas

NOTICES

Disclaimers

The findings in this report are not to be construed as an official Department of the Army position unless so designated by other authorized documents.

Citation of manufacturer's or trade names does not constitute an official endorsement or approval of the use thereof.

Destroy this report when it is no longer needed. Do not return it to the originator.

ARL-TR-9567 ● SEP 2022

The T5 Isochronal Age-Hardening Response of As-Solidified Mg–Li–RE–(Al) Alloys

Taylor Cain and Joseph Labukas
DEVCOM Army Research Laboratory

REPORT DOCUMENTATION PAGE

Form Approved
OMB No. 0704-0188

1. REPORT DATE *(DD-MM-YYYY)*	2. REPORT TYPE	3. DATES COVERED (From - To)
September 2022	Technical Report	1 November 2021–1 July 2022

4. TITLE AND SUBTITLE
The T5 Isochronal Age-Hardening Response of As-Solidified Mg–Li–RE–(Al) Alloys

5a. CONTRACT NUMBER

5b. GRANT NUMBER

5c. PROGRAM ELEMENT NUMBER

6. AUTHOR(S)
Taylor Cain and Joseph Labukas

5d. PROJECT NUMBER

5e. TASK NUMBER

5f. WORK UNIT NUMBER

7. PERFORMING ORGANIZATION NAME(S) AND ADDRESS(ES)
DEVCOM Army Research Laboratory
ATTN: FCDD-RLW-MF
Aberdeen Proving Ground, MD 21005

8. PERFORMING ORGANIZATION REPORT NUMBER
ARL-TR-9567

9. SPONSORING/MONITORING AGENCY NAME(S) AND ADDRESS(ES)

10. SPONSOR/MONITOR'S ACRONYM(S)

11. SPONSOR/MONITOR'S REPORT NUMBER(S)

12. DISTRIBUTION/AVAILABILITY STATEMENT
Approved for public release: distribution unlimited.

13. SUPPLEMENTARY NOTES
ORCID ID: Taylor Cain, 0000-0002-6621-914X

14. ABSTRACT
This investigation sought to explore the age hardenability of Mg–Li–RE–(Al) alloys where RE = Gd, Y, Nd. Alloys were made by induction melting and furnace cooling. The resulting as-solidified alloys were subjected to isochronal heat treatment of 2 h at temperatures between 150–400 °C followed by water quenching. Hardness measurements revealed Mg–Li–RE alloys containing Al displayed a U-shaped age-hardening effect where the hardness was large at low and high temperatures but decreased at intermediate temperatures. On the contrary, Mg–Li–RE alloys sans Al did not show an age-hardening response, likely due to precipitation of RE-rich phases upon solidification. Correlations of hardness with historical tensile data of Mg–Li alloys indicate that Mg–Li–RE alloys are not likely to be considered for structural applications.

15. SUBJECT TERMS
Mg–Li alloy, age hardening, precipitation hardening, rare earth, Sciences of Extreme Materials

16. SECURITY CLASSIFICATION OF:			17. LIMITATION OF ABSTRACT	18. NUMBER OF PAGES	19a. NAME OF RESPONSIBLE PERSON
a. REPORT	b. ABSTRACT	c. THIS PAGE			Taylor Cain
Unclassified	Unclassified	Unclassified	UU	23	19b. TELEPHONE NUMBER (Include area code) (410) 278-3162

Standard Form 298 (Rev. 8/98)
Prescribed by ANSI Std. Z39.18

Contents

List of Figures

1. Introduction

Magnesium–lithium (Mg–Li) alloys are of great interest due to their low density (1.3–1.65 g/cm^3), high specific strengths, and ability to form a body-centered cubic (BCC) matrix, which provides greater ductility and formability than conventional hexagonal close-packed (HCP) Mg alloys.[1,2] The development of Mg–Li alloys for structural applications dates to the 1940s where extensive efforts were made in the United States and former Soviet Union until the 1980s.[1,3–9] During this period, several alloys were developed for commercial application, but new alloy development efforts faltered due to the lack of thermomechanical stability of high-strength alloys based on ternary aluminum (Al), zinc (Zn), silver (Ag), and cadmium (Cd) additions at temperatures below 100 °C. However, there has been a rejuvenated interest in Mg–Li alloy development to explore the origins of thermomechanical instability in BCC Mg–Li–Al-based alloys using high-fidelity characterization techniques that did not exist until recent times.[10–13] These efforts have been further stimulated by the development of a high specific strength, so-called "stainless" Mg alloy.[13] While much of the development work on Mg–Li alloys, including focus on corrosion resistance, has been summarized in recent literature,[14–16] there remains a paucity of research investigating the effect of rare earth (RE) element alloy additions with atomic numbers greater than 60 to the strengthening and corrosion behavior of BCC Mg–Li alloys.

The goal of this research was to explore the hardening response of BCC Mg–Li alloys containing gadolinium (Gd), yttrium (Y), and neodymium (Nd) in various combinations with and without Al. Gd was chosen as we could find no studies to date in the literature on the precipitation hardenability of BCC Mg–Li with Gd in addition to the combination of Gd with other RE elements and Al. Similarly, we could not find any data for BCC Mg–Li with the combination of Y and Nd but HCP Mg alloys have shown excellent precipitation hardening responses for Mg–Gd–(Y)[17,18] and Mg–Y–Nd[19]-based alloys. To explore the hardening response, isochronal heat treatments were performed between 150–400 °C from the as-solidified condition to mimic a T5 heat treatment. An isochronal anneal was chosen as it represents an efficient method for finding a temperature range for age hardening when precipitation behavior is unknown.

2. Experimental Procedures

Alloys were prepared using 99.9% Mg–22Li, Mg–30Gd, and Mg–25Y master alloys in weight percent (American Elements), 99.95% Al shot (Belmont Metals), 99.95% Mg ingot (US Magnesium), commercial Mg alloys E675 and WE43

(Magnesium Elektron), and 99.99% Li rod (Alfa Aesar). For this investigation, the following alloys were targeted in weight percent:

- Mg-14Li-0.87Gd (LG141)
- Mg-14Li-0.87Gd-0.24Y (LGY1410)
- Mg-14Li-3Al-0.87Gd (LAG1431)
- Mg-14Li-5.6Gd-4.8Y-0.3Zr (LE675)
- Mg-14Li-3Al-3.5Y-2.6Nd-0.5Zr-0.3Ge (HGM)

Alloys LE675 and HGM were prepared using pure Li, Al, and germanium (Ge) additions to commercial Mg alloys E675 and WE43.

Two separate furnaces were used for making alloys. First, the necessary components for LE675 and HGM were placed in a 250-mL stainless-steel beaker coated in boron nitride (BN; ZYP Coatings) and subsequently loaded into a quartz tube within an argon (Ar)-filled glovebox. The quartz tube was sealed with a vacuum flange assembly, as shown in Fig. 1, and removed from the glove box for melting with a 25-kW vacuum induction melting (VIM) furnace possessing an output frequency of 30–80 kHz (MTI Corporation). The vacuum flange assembly was connected to a flow of ultra-high purity (UHP; 99.999%) helium (He) gas under a slight positive pressure to mitigate oxidation of the melt. The alloy charge was melted at approximately 685 °C for 5 min to provide initial mixing of Li and allowed to furnace cool. The resulting solidified alloys of LE675 and HGM were re-melted in a different induction furnace.

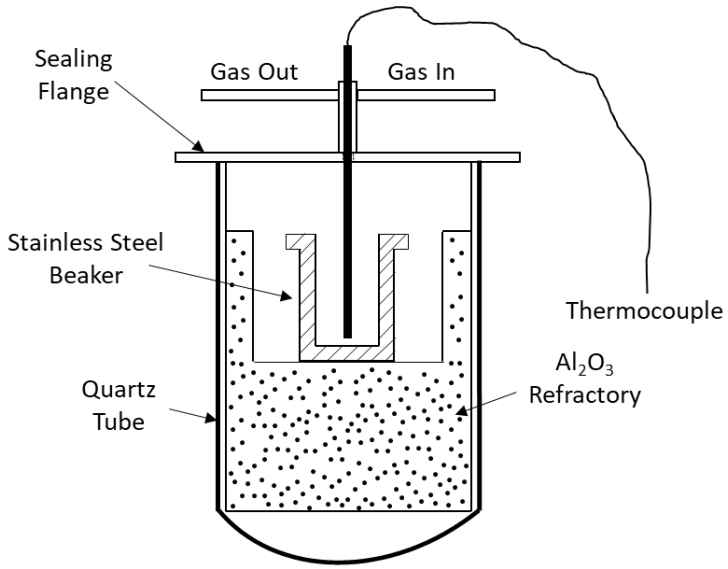

Fig. 1 Quartz tube and vacuum flange assembly used for alloys requiring additions of pure Li

Final preparation of all alloys was performed using the Blue Power VTC 800 V/Ti vacuum induction furnace. The 100-mL stainless-steel beaker coated with BN contained the desired alloy charge for approximately 35 g of total alloy mass and was placed inside a graphite crucible in the induction furnace chamber. Prior to melting, the furnace was placed under vacuum to a pressure below 1 mbar and backfilled with UHP He five times to provide an inert gas atmosphere. The alloy charge was melted under a He environment at atmospheric pressure at a temperature of 685 °C using an S-type thermocouple sheathed in 304 stainless steel. The melt was held for 15 min to ensure mixing of all elements and then allowed to furnace cool. Alloys were then allowed to stabilize for 6 months prior to further testing to allow for any natural ageing effects.

The as-solidified alloys were evaluated for their ability to precipitation-harden using isochronal steps of 2 h ranging from 150–400 °C and water quenching. Heat treatments were performed in a muffle furnace without protective gas flow; 400 °C was chosen as the highest temperature due to flammability concerns. Alloys were coated in BN prior to heat treatment to reduce oxidation of the alloys. Samples from each heat treatment were ground and polished immediately after water quenching and polished to a 0.25-µm finish using silicon carbide (SiC) grinding paper and diamond glycol-based polishing solutions. Micro Vickers hardness measurements using a Mitutoyo HM-200 were performed using a 0.3-kg load with a load time of 5 s, dwell time of 10 s, and unload time of 5 s. Selected samples based on hardness measurements were evaluated using scanning electron microscopy (SEM; Hitachi SU3500) equipped with a Bruker QUANTAX energy dispersive spectroscopy (EDS) detector. EDS maps were generated using K radiation peaks for oxygen (O), Mg, Al, and Ge while L_α peaks were used for RE elements to avoid false signals from low energy M peaks with the K peak shoulders associated with O, Mg, and Al. Note that Li cannot be detected by EDS. Additional hardness measurements were made using the Rockwell E (HRE) scale for comparison to historical Mg–Li alloys.

3. Results and Discussion

3.1 SEM Microscopy of As-Solidified Alloys

3.1.1 Mg–Li–RE Alloys

Representative backscattered election (BSE) images of each alloy with accompanying EDS maps are shown in Figs. 2–6. BSE imaging of LG141 revealed the presence of small second-phase particles (<10 µm) given by the bright contrast in the BSE image of Fig. 2. These particles were uniformly dispersed throughout

the alloy. The corresponding signal of these particles are associated with Gd, thus indicating they are Gd-rich particles. Additional O-rich particles can be observed, which likely formed on the surface during the time after completion of the final polishing and before introduction into the SEM. Bright particles similar to those found in LG141 are found in the BSE image of LGY1410, as shown in Fig. 3, where two different sizes of particles are observed. Small, sub-micrometer particles are observed throughout the matrix, while also being found along a grain boundary in the vertical midline of the image. However, there is a wide precipitate-free zone along the grain boundary approximately 10–20 μm in width, likely indicating depletion of Gd as Gd can be associated with the bright particles along the grain boundary. Additional Gd- and Y-rich particles are observed as being the largest particles present in LGY1410. The final alloy without Al additions was LE675, whose characteristic BSE image and EDS mapping is shown in Fig. 4. Here, a lamellar secondary phase rich with Gd and Y can be observed, indicating hypoeutectic solidification.

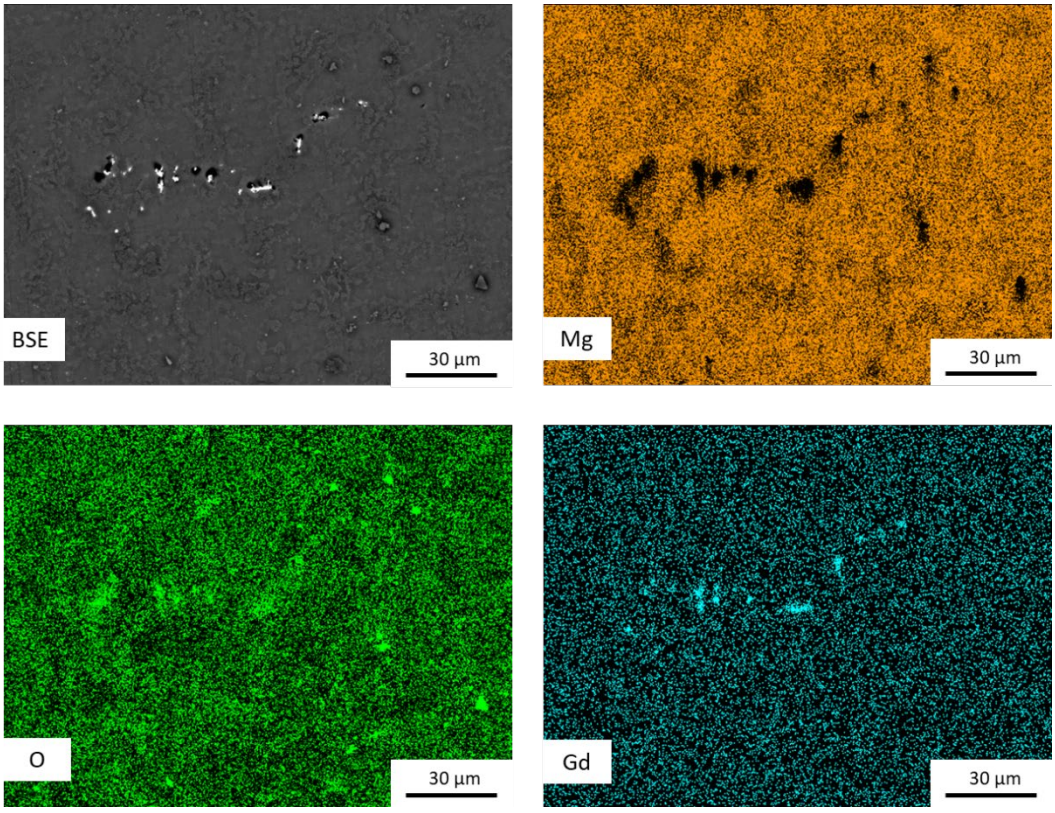

Fig. 2 Representative BSE image (top left) and EDS maps for as-solidified LG141

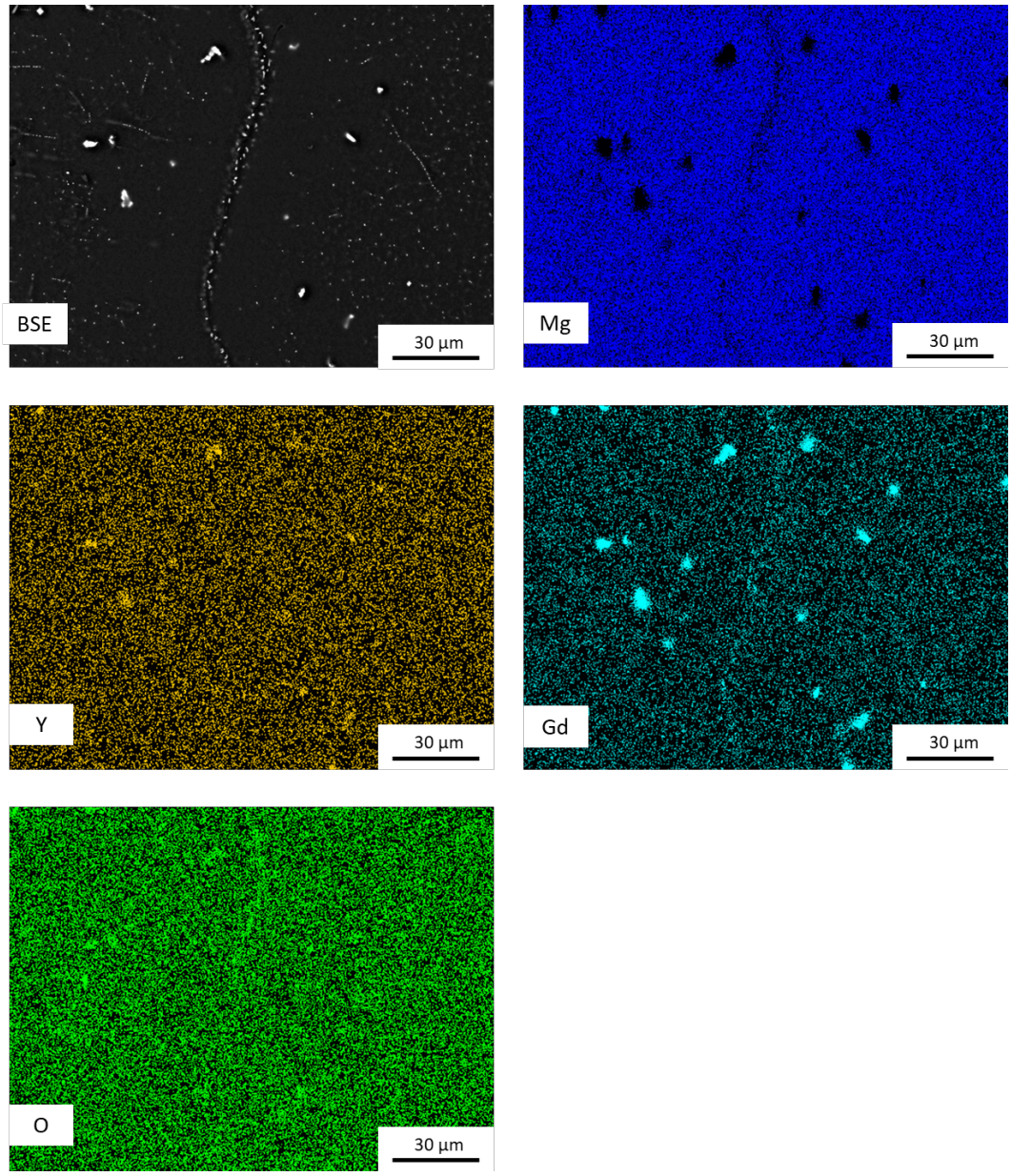

Fig. 3 Representative BSE image (top left) and EDS maps for as-solidified LGY1410

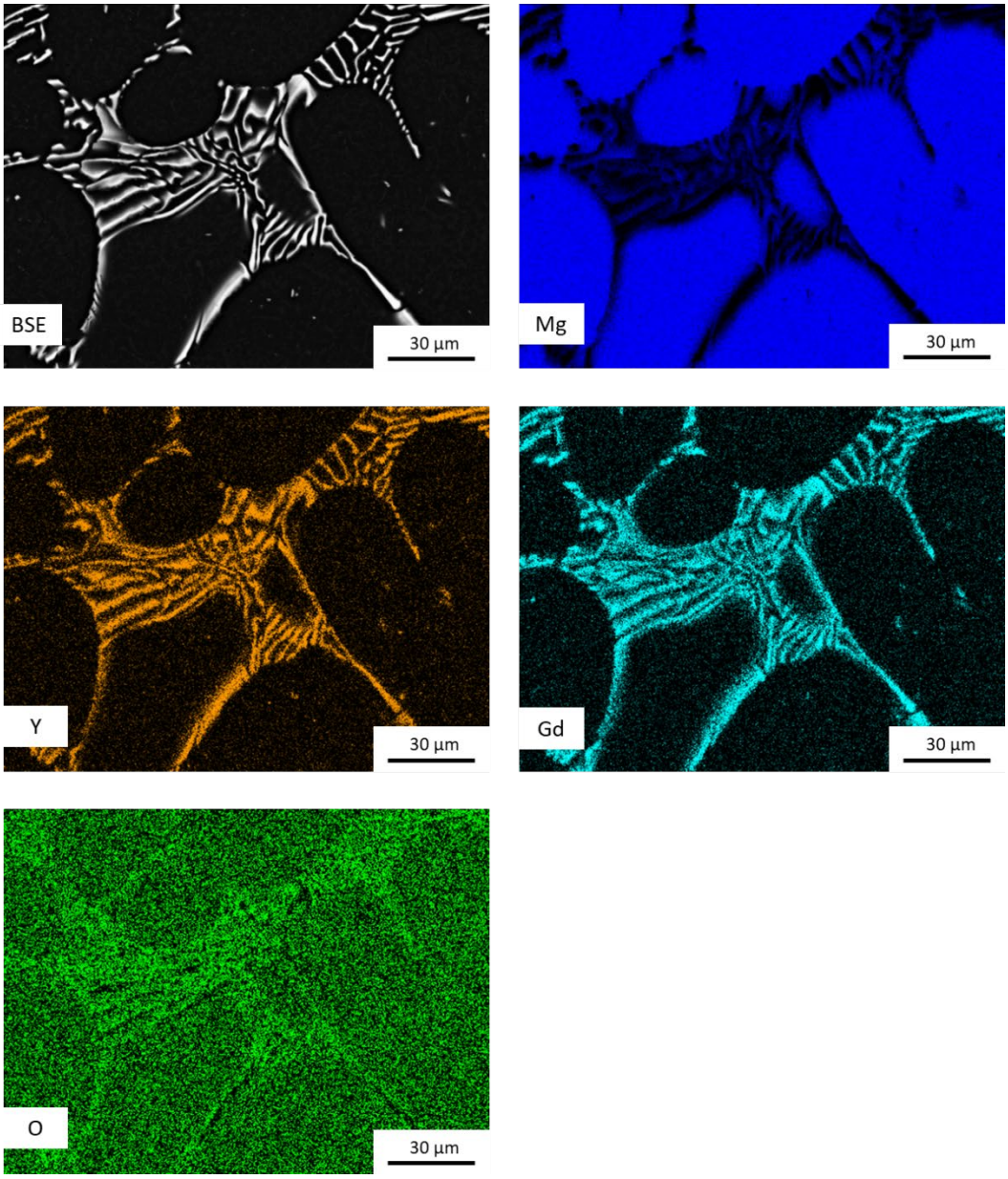

Fig. 4 Representative BSE image (top left) and EDS maps for as-solidified LE675

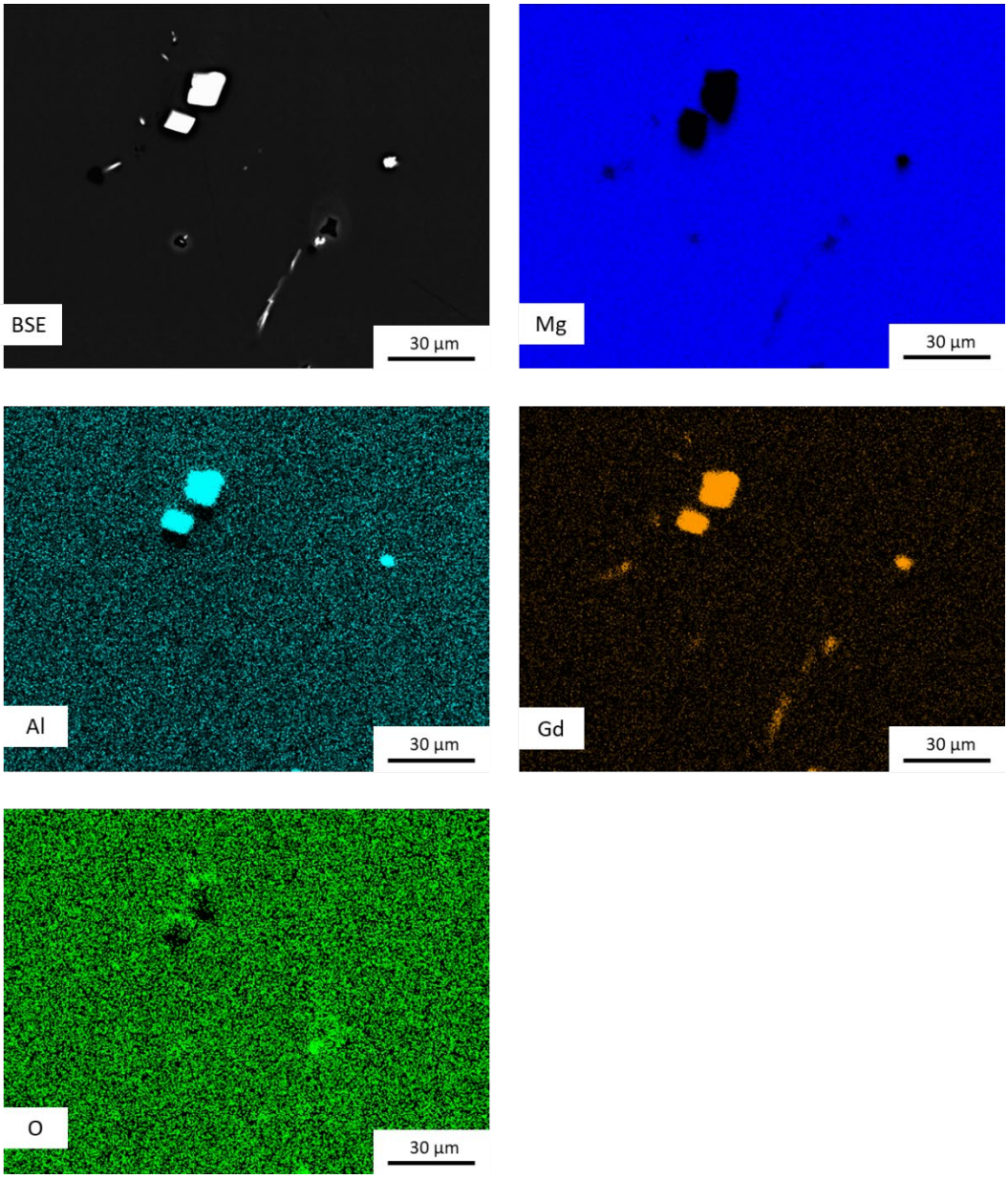

Fig. 5 Representative BSE image (top left) and EDS maps for as-solidified LAG1431

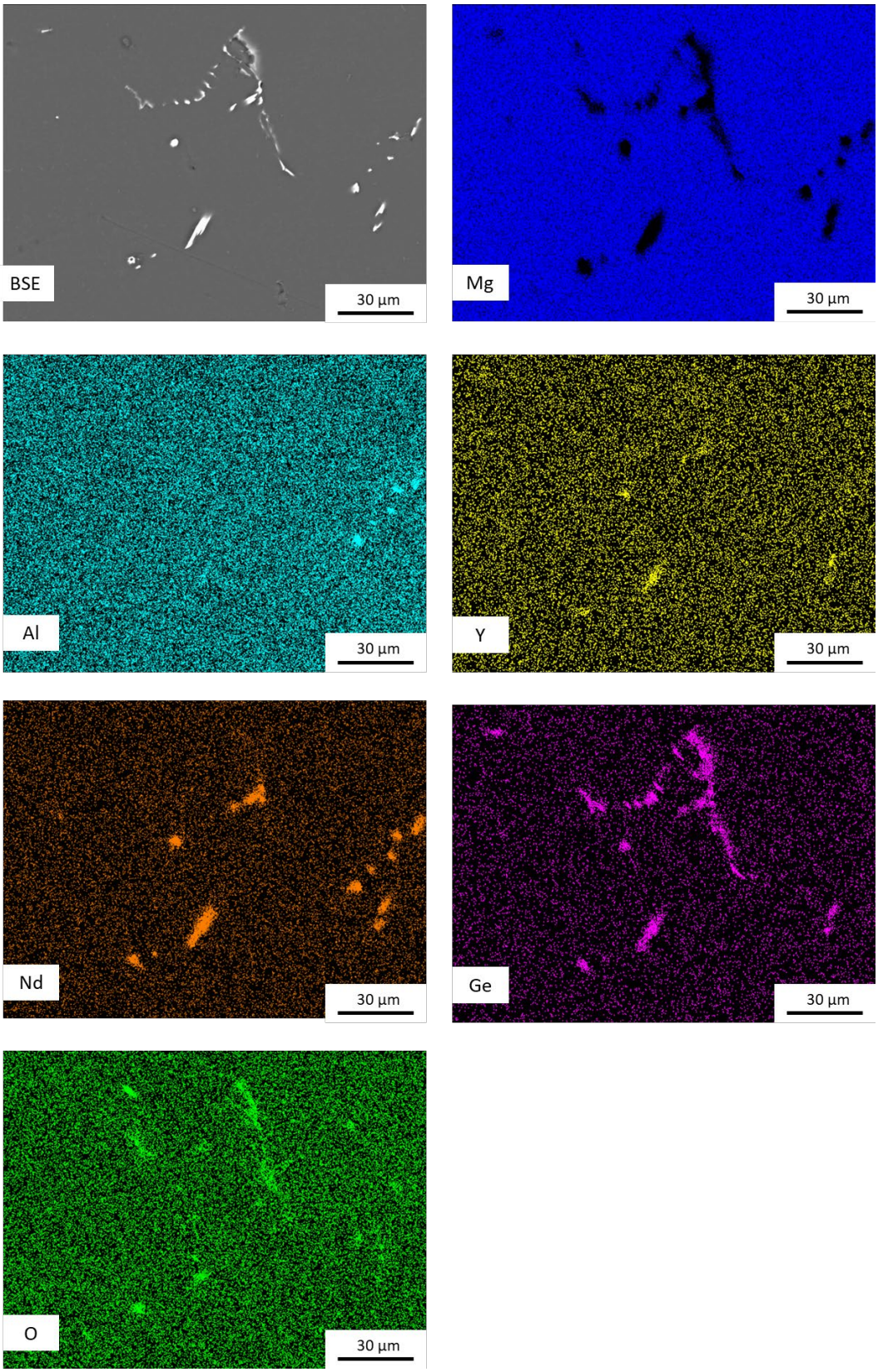

Fig. 6 Representative BSE image (top left) and EDS maps for as-solidified HGM

3.1.2 Mg–Li–RE–Al Alloys

The characteristic microstructure of LAG1431 is shown in Fig. 5, where a large blocky phase can be observed with some smaller secondary-phase particles. The larger particles present are rich in both Al and Gd, while some smaller Gd-rich particles indicate competitive phase formation between the (Al, Gd)-rich phase and the Gd-rich phase upon solidification and cooling. For HGM, several different phase morphologies were observed including blocky phases and a lamellar-type phase. The blocky phases were mostly associated with Nd and Y while others were rich in Al and Nd. Interestingly, Ge was found to correlate with the (Nd, Y)-rich phase in addition to the lamellar phase. The lamellar phase, as with LE675, indicates hypoeutectic solidification owing to the low-solubility Ge in ß-Li.[20]

3.2 Isochronal Age Hardening

A plot of the isochronal data of hardness is shown in Fig. 7 for micro Vickers hardness (Fig. 7a) and HRE (Fig. 7b). These figures reveal that the measured hardness was relatively constant for non-Al-containing alloys, which indicates that precipitation hardening did not occur from the as-solidified condition. This is likely because the precipitation of available RE solute upon solidification in secondary phases provides little resistance to dislocation motion. As such, precipitation hardenability of these alloys may benefit from solution treatment and ageing as opposed to ageing from the as-solidified condition. In contrast, the hardness of the Al-containing alloys was high in the as-solidified condition and then decreased with increasing temperatures up to 300 °C where a minimum occurred; the hardness then increased to values similar to that of the as-solidified value, which is likely due to the rapid nucleation and growth of Al-containing nano precipitates. This quench sensitivity is well known for BCC Mg–Li–Al-based alloys and would agree with the results found by Ferry and co-workers.[11–13] Their recent work studying the precipitation-hardening response of an Mg–10.95Li–3.29Al–0.19Zr–0.59Y alloy (LA113) with synchrotron diffraction has indicated that the high hardening response below about 125 °C is due to the formation of Al-rich clusters upon quenching while the θ ($D0_3$−Mg_3Al) phase forms between the range of about 125−275 °C. Next, the spinodal decomposition of θ to the equilibrium Al–Li phase was cited between about 275−325 °C. Finally, at temperatures above 325 °C, solutionizing of precipitates to the ß-phase is observed and the corresponding room-temperature hardness was a result of formation of Al-rich clusters upon quenching. As this precipitation sequence involves only Mg, Li, and Al, it is likely that a similar type of reaction sequence occurs in both LAG143 and HGM, which have a similar concentration of Al. This assertion is further strengthened by the observation that RE-containing phases did not provide a hardening response in Al-free alloys.

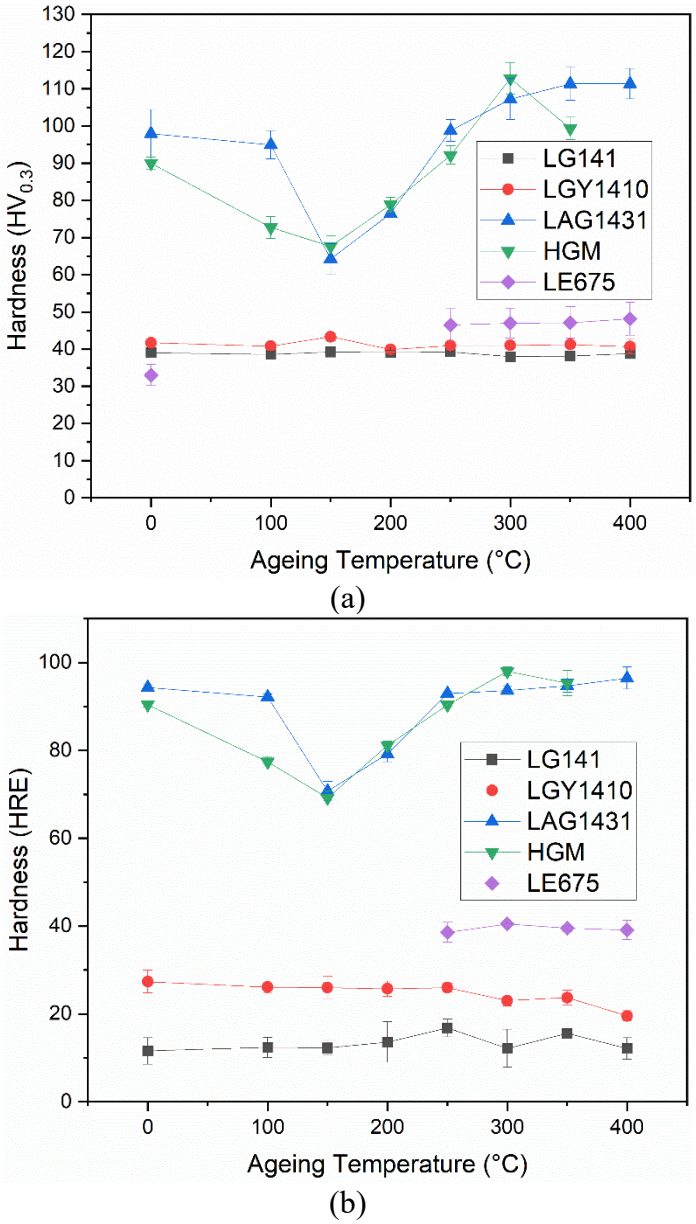

Fig. 7 The average measured hardness values of 2 h isochronal heat treatment for (a) micro Vickers hardness and (b) HRE in comparison to notable Mg–Li alloys

The relationship between HRE and micro Vickers hardness is plotted in Fig. 8. This data was fit using an exponential regression equation via the Levenberg−Marquardt algorithm with the OriginPro 2020 software program. Also included in the fit is the 95% confidence interval, which represents uncertainty in the fit data, and the 95% prediction band, which represents the uncertainty about a new data point being added to the curve. The resulting fit is given in Eq. 1 and showed an excellent correlation with a Pearson R^2 value of 0.994 (R^2 = 1 indicates a perfect fit). This relationship is useful for comparing the measured hardness values of archival Mg–

Li data, which was measured using HRE whereas contemporary studies use Vickers hardness. In a similar manner, attempts to correlate HRE with measured yield strength (YS) and ultimate tensile strength (UTS) of Mg–Li alloys are given in Figs. 9 and 10, respectively, using the extensive data of Frost et al.[3] The Pearson R^2 values of these plots were 0.761 for YS and 0.7 for UTS, indicating a positive correlation but not as strong as that for the fit in Fig. 8. However, the 95% prediction band can be useful in estimating a range for the mechanical property response. With this in mind, the Al-free alloys whose hardness values were less than or equal to about 40 HRE would be projected to have YSs lower than 100 MPa and UTS below 150 MPa. These values are very low in comparison to high-strength Mg alloys and would not make the minimum requirements for Mg armor under MIL-DTL-32333.[21] Conversely, high hardness alloys LAG141 and HGM are promising materials, but it is not clear how much benefit the RE additions provide to broad mechanical property response and corrosion resistance. Further research needs to be conducted on Mg–Li–Al–RE alloys to determine the effects of the Al_xRE_y precipitates that form upon solidification.

$$HRE = -369.959 \times e^{-\frac{HV}{26.774}} + 102.186,\ R^2 = 0.994 \qquad (1)$$

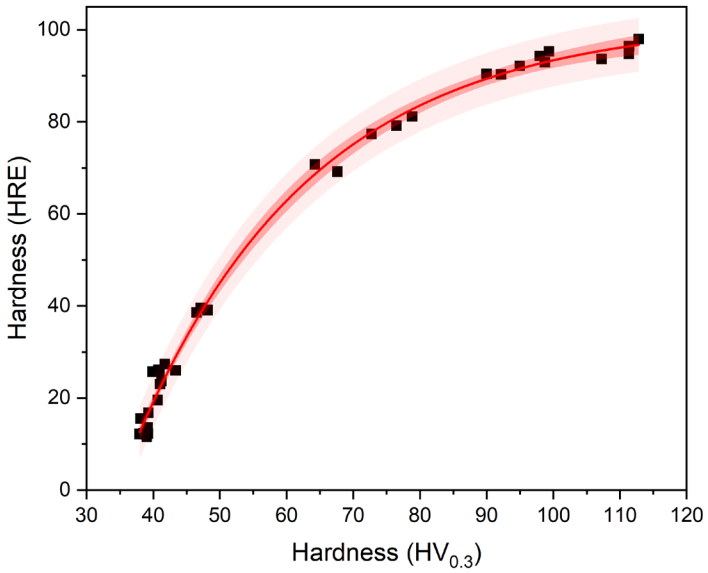

Fig. 8 Plot of Vickers hardness vs. HRE for the alloys tested

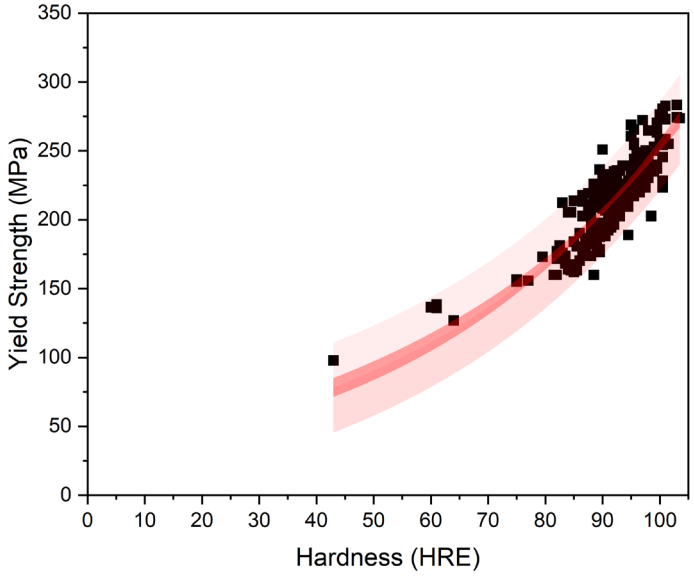

Fig. 9 Plot of YS as a function of HRE for Mg–Li alloys from Frost et al.[3] with the 95% confidence band in dark pink and the 95% prediction band in light pink

$$YS = 32.24 \times e^{0.0206HRE},\ R^2 = 0.761 \quad (2)$$

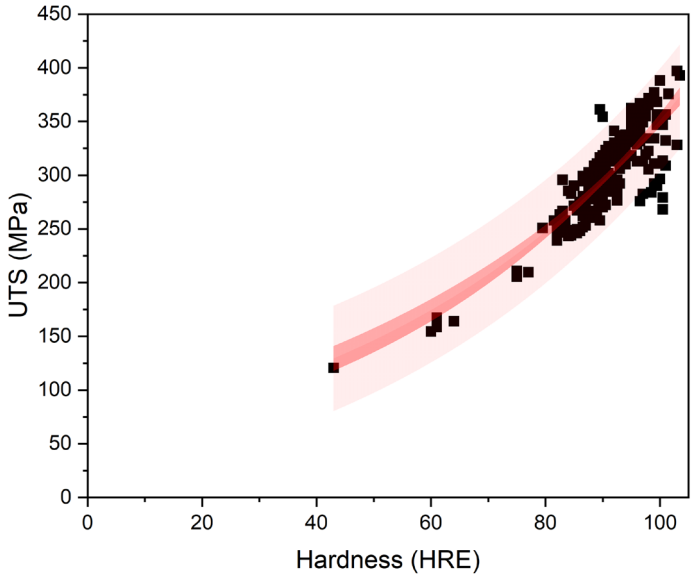

Fig. 10 Plot of UTS as a function of HRE for Mg–Li alloys from Frost et al.[3] with the 95% confidence band in dark pink and the 95% prediction band in light pink

$$UTS = 61.02 \times e^{0.0175HRE},\ R^2 = 0.700 \quad (3)$$

4. Conclusion and Recommendations

BCC Mg–Li–Al–RE-based alloys displayed greater hardening response than Mg–Li–RE alloys in the as-solidified and heat-treated condition, likely due to the formation of Al-rich nanoprecipitates. Additional heat treatments are needed to determine solutionizing times and temperatures for Mg–Li–RE alloys for possible T6 heat treatment.

RE additions to BCC Mg–Li resulted in large, blocky RE-rich precipitates that provided little hardening response. RE additions in Mg–Li–Al alloys tended to form Al–RE rich precipitates.

Additional research is needed to determine the effects of RE elements in Mg–Li–Al alloys on the corrosion response and other critical material properties.

5. References

1. Jackson JH, Frost PD, Loonam AC, Eastwood LW, Lorig CH. Magnesium–lithium base alloys—preparation, fabrication, and general characteristics. JOM. 1949;1:149–168.
2. Kamado S, Kojima Y. Deformability and strengthening of superlight Mg–Li alloys. Metall Sci Technol. 1998;16(1).
3. Frost PD, Whittenburg RV, Kura JG, Eastwood LW. The development of magnesium–lithium base alloys for armor plate. Report to Bureau of Aeronautics, Contract NOa(s) 9526, Battelle Memorial Institute; 1950.
4. Raynor GV, Butchers E. Equilibrium relations and some properties of magnesium lithium and magnesium silver lithium alloys. J Inst Met. 1945;71:589–601.
5. Busk RS, Leman DL, Casey JJ. The properties of some magnesium–lithium alloys containing aluminum and zinc. JOM. 1950;2:945–951.
6. Frost P, Jackson J, Loonam A, Lorig C. The effect of sodium contamination on magnesium–lithium base alloys. JOM. 1950;2(9):1171–1172.
7. Frost P, Kura J, Eastwood L. Aging characteristics of magnesium–lithium base alloys. JOM. 1950;2:1277–1282.
8. Drits MY, Sviderskaya ZA, Yelkin FM, Trokhova VF. Superlight structural alloys [in Russian]; 1972.
9. Drits MY, Yelkin FM, Gur'yev II, Bondaryev BI, Trokhova VF, Sergiyevskaya AD, Osokina TN. Magnesium–lithium alloys [in Russian]; 1980.
10. Tang S, Xin T, Xu W, Miskovic D, Sha G, Quadir Z, Ringer S, Nomoto K, Birbilis N, Ferry M. Precipitation strengthening in an ultralight magnesium alloy. Nat Commun. 2019;10:1003.
11. Xin T, Tang S, Ji F, Cui L, He B, Lin X, Tian X, Hou H, Zhao Y, Ferry M. Phase transformations in an ultralight BCC Mg alloy during anisothermal ageing. Acta Materialia. 2022;239:118248.
12. Xin T, Zhao Y, Mahjoub R, Jiang J, Yadav A, Nomoto K, Niu R, Tang S, Ji F, Quadir Z, et al. Ultrahigh specific strength in a magnesium alloy strengthened by spinodal decomposition. Sci Adv. 2021;7(23):eabf3039.

13. Xu W, Birbilis N, Sha G, Wang Y, Daniels JE, Xiao Y, Ferry M. A high-specific-strength and corrosion-resistant magnesium alloy. Nat Mater. 2015;14:1229–1235.

14. Cain TW, Labukas JP. The development of β phase Mg–Li alloys for ultralight corrosion resistant applications. npj Mater Degrad. 2020;4:17.

15. Wu R, Yan Y, Wang G, Murr LE, Han W, Zhang Z, Zhang M. Recent progress in magnesium–lithium alloys. Int Mater Rev. 2014;60:65–100.

16. Sun Y-h, Wang R-c, Peng C-q, Yan F, Ming Y. Corrosion behavior and surface treatment of superlight Mg–Li alloys. T Nonferr Metal Soc China. 2017;27(7):1455–1475.

17. Wang D, Li D, Xie Y, Zeng X. HRTEM studies of aging precipitate phases in the Mg-10Gd-3Y-0.4Zr alloy. J Rare Earth. 2016;34:441–446.

18. Rokhlin LL. The regularities in the Mg-rich parts of the phase diagrams, phase transformation and mechanical properties of Mg alloys with individual rare earth metals. Arch Metall Mater. 2007;52:1–7.

19. Lussana D, Massazza M, Riontino G. A DSC study of precipitation hardening in a WE43 Mg alloy. J Therm Anal Calorim. 2008;92:223–225.

20. Cain TW, Labukas JP. Development of ultra lightweight, corrosion resistant Mg alloys. In: Jordon JB, Miller V, Joshi VV, Neelameggham NR, editors. Magnesium Technology 2020. Springer, Cham; c2020. p. 43–48.

21. MIL-DTL-32333. Armor plate, magnesium alloy, Az31B, WE43C, applique. Naval Publications and Form Center; 2020 Sep 11.

List of Symbols, Abbreviations, and Acronyms

Ag	silver
Al	aluminum
Ar	argon
BCC	body-centered cubic
BN	boron nitride
BSE	backscattered election
Cd	cadmium
EDS	energy dispersive spectroscopy
Gd	gadolinium
Ge	germanium
HCP	hexagonal close packed
He	helium
HRE	Rockwell E scale hardness
Mg–Li	magnesium–lithium
Nd	neodymium
O	oxygen
RE	rare earth
SEM	scanning electron microscopy
SiC	silicon carbide
UHP	ultra-high purity
UTS	ultimate tensile strength
VIM	vacuum induction melting
Y	yttrium
YS	yield strength
Zn	zinc

1 (PDF)	DEFENSE TECHNICAL INFORMATION CTR DTIC OCA
1 (PDF)	DEVCOM ARL FCDD RLD DCI TECH LIB
2 (PDF)	DEVCOM ARL FCDD RLW MF T CAIN J LABUKAS